GA–A23159

# DIVERTOR E$\times$B PLASMA CONVECTION IN DIII–D

by
J.A. BOEDO, M.J. SCHAFFER, M. MAINGI,
C.J. LASNIER, and J.G. WATKINS

JULY 1999

# DISCLAIMER

GA–A23159

# DIVERTOR E$\times$B PLASMA CONVECTION IN DIII–D

by
J.A. BOEDO,* M.J. SCHAFFER, M. MAINGI,†
C.J. LASNIER,‡ and J.G. WATKINS△

This is a preprint of a paper presented at the Twenty-Sixth European Physical Society Conference on Controlled Fusion and Plasma Physics, June 14–18, 1999 in Maastricht, The Netherlands, and to be published in *The Proceedings.*

*University of California, San Diego, California.
†Oak Ridge National Laboratory, Oak Ridge, Tennessee.
‡Lawrence Livermore National Laboratory, Livermore, California.
△Sandia National Laboratories, Albuquerque, New Mexico.

Work supported by
the U.S. Department of Energy
under Contract Nos. DE-AC03-99ER54463, DE-AC05-96OR22464,
W-7405-ENG-48, DE-AC04-94AL85000, and Grant No. DE-FG03-95ER54294

GA PROJECT 30033
JULY 1999

# Divertor E×B Plasma Convection in DIII-D

J.A. Boedo,[1] M.J. Schaffer, R. Maingi,[2] C.J. Lasnier,[3] J.G. Watkins[4]

*General Atomics, P.O. Box 85608, San Diego, California 92186-5608*

*[1]University of California – San Diego, San Diego, California.*
*[2]Oak Ridge National Laboratory, Oak Ridge, Tennessee.*
*[3]Lawrence Livermore National Laboratory, Livermore, California.*
*[4]Sandia National Laboratories, Albuquerque, New Mexico.*

**Abstract.** Extensive two-dimensional measurements of plasma potential in the DIII–D tokamak divertor region are reported for standard (ion $\nabla B_T$ drift toward divertor X–point) and reversed $\mathbf{B}_T$ directions; for low (L) and high (H) confinement modes; and for partially detached divertor mode. The data are consistent with recent computational modeling identifying $\mathbf{E}\times\mathbf{B}_T$ circulation, due to potentials sustained by plasma gradients, as the main cause of divertor plasma sensitivity to $\mathbf{B}_T$ direction.

## Introduction

The function of a magnetic divertor is to provide heat and particle exhaust and shield the main plasma from impurity contamination. Heat and particles are transported from the plasma core to the edge and SOL plasma, whence particles are convected and heat is both conducted and convected to the divertor target. The SOL transport is mainly parallel to the magnetic field **B**.

An outstanding question is the long-observed asymmetry in the power and particle fluxes between the inner and outer divertor targets and its strong dependence on the direction of the toroidal magnetic field $\mathbf{B}_T$ [1]. Inner and outer target power fluxes differ by factors of five or more with standard $\boldsymbol{B}_T$ direction, yet the difference can nearly disappear with reversed $\boldsymbol{B}_T$. It has been hypothesized that this asymmetry arises in some way from the $\mathbf{B}\times\nabla B/B^2$ and $\mathbf{E}\times\mathbf{B}/B^2$ particle drifts. Recent numerical calculations with the UEDGE plasma and gas edge simulation code, including all the classical particle drifts, reproduce the main features of the in–out asymmetry dependence on $B_T$ direction [2]. By enabling and disabling the various drift terms in the code, the $\mathbf{E}\times\mathbf{B}_T$ drift was identified as dominant, in agreement with an earlier prediction [3]. We report two-dimensional measurements of divertor electric potentials that confirm the magnitude of divertor $\mathbf{E}\times\mathbf{B}_T$ flows.

## Experimental Arrangement

The experiments were carried out in the DIII–D tokamak with plasma current $I_p$ = 1.4 MA and $B_T = \pm 2$ T at $R_0$ = 1.7 m. The neutral beam heating power varied from 0.5 to 8.75 MW during the discharge, producing L–mode and H–mode phases. The single-null divertor was in the bottom of the vacuum vessel, which is instrumented for divertor studies [4].

The principal measurements were made by a fast reciprocating probe featuring five tips to measure ion saturation current, $T_e$, $n_e$, floating potential $\Phi_f$ and the parallel plasma Mach number in the divertor. The plasma potential $\Phi_p$ is calculated from $\Phi_f$ and $T_e$. The probe scans vertically from the target in approximately 250 ms along a path at major radius $R$ = 1.486 m. The divertor Thomson scattering system, also at $R$ = 1.486 m, provided independent $T_e$ and $n_e$ measurements every 50 ms at 8 vertical locations separated by 15–30 mm. The divertor plasma was stepped radially by changing the external equilibrium magnetic field to obtain 2-D measurements over much of the divertor region Fig. 1(a) inset. Data taken along several vertical probe insertions are mapped on to magnetic surfaces calculated by the toroidal equilibrium fitting code EFIT [5] to form a composite plot. Surfaces are labeled by their normalized poloidal magnetic flux, $\psi_n$: the separatrix is at $\psi_n = 1$; the SOL has $\psi_n > 1$ increasing away from the separatrix; and $\psi_n < 1$ is either private region or "core" plasma with $\psi_n$ decreasing away from the separatrix.

## Results

Results for the outer SOL region of attached–divertor, ELMing H–mode discharges for standard $B_T$ direction are shown in Fig.1. The plotted data are composed from the outer four probe trajectories in the Fig. 1 inset. The data overlay well, confirming that parallel gradients are negligible over the selected region. The potential gradients yield the electric field normal to the surfaces. The plasma potential $\Phi_p$ Fig. 1(a) rises by ~200 V in 40–50 mm (5 kV/m) across the separatrix, from the cold private region to the hot SOL, and decreases outward through the SOL (~1 kV/m). The inner SOL potential distribution (not shown) is nearly the same as the outer over the region that could be measured.

The potential "well" just outside the separatrix in Fig. 1(a), a reproducible outer leg feature, is semiquantitatively consistent with the $\eta_{\|}J_{\|}$ Ohmic potential drop of the measured electric current to the target, which is of thermoelectric and Pfirsch–Schlüter origin [6]. The well introduces large opposing gradients (7 kV/m) and an unanticipated local velocity shear layer.

The potential distributions with reversed $\mathbf{B}_T$, Fig. 2, are similar to those with standard $\mathbf{B}_T$. They have the same sign and magnitude, but all the reversed $\mathbf{B}_T$ profiles are shifted somewhat away from the separatrix, as predicted by the computation [2].

L–mode attached–divertor discharges not shown, had potential distributions similar to H–mode, but the magnitude of the separatrix potential drop was lower, ~125 V.

Potential and density profiles vs. height from the target in the outer leg during two partially detached divertor (PDD) discharges are shown in Fig. 3. Note that the potential gradients are much smaller than in attached discharges. However, because the plasma density is ~20 times greater, the $\mathbf{E}\times\mathbf{B}_T$ particle convection is still comparably large.

The measured divertor electric fields create $\mathbf{E}\times\mathbf{B}_T$ convection as sketched in Fig. 4. We call attention to the $\mathbf{E}\times\mathbf{B}_T$ flow along the private side of the separatrix, ignored until recently [2], that strongly couples the outer and inner divertors.

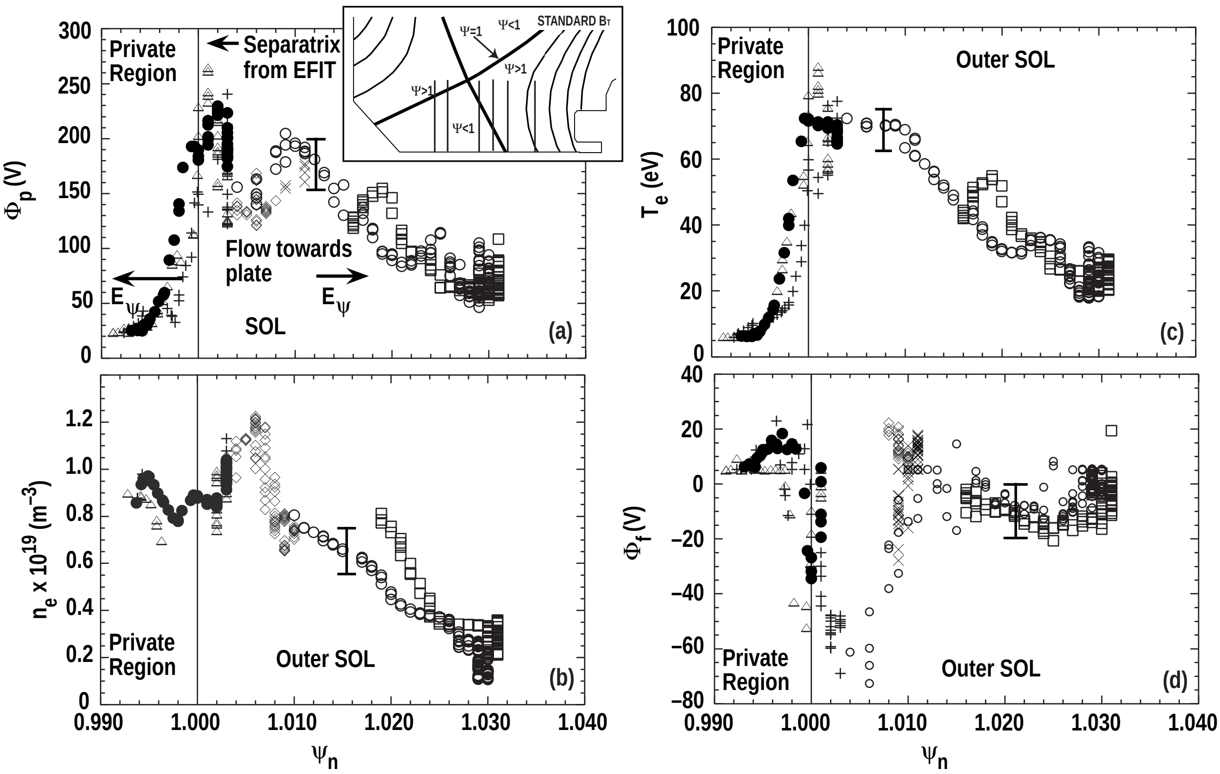


FIG. 1. Measured profiles of (a)$\Phi_p$, (b) $n_e$, (c) $T_e$, and (d) floating potential, $\Phi_f$, in the outer divertor leg as a function of $\psi_n$ for standard $B_T$ direction. Inset shows probe trajectories schematically in these ELMing H–mode plasmas.

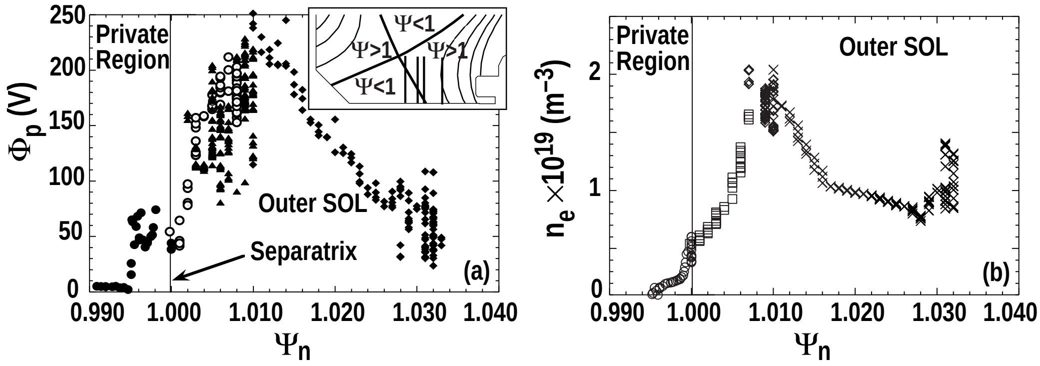


FIG. 2. Measured profiles of (a) $\Phi_p$ and (b) $n_e$ for reversed $B_T$, attached, H–mode plasmas.

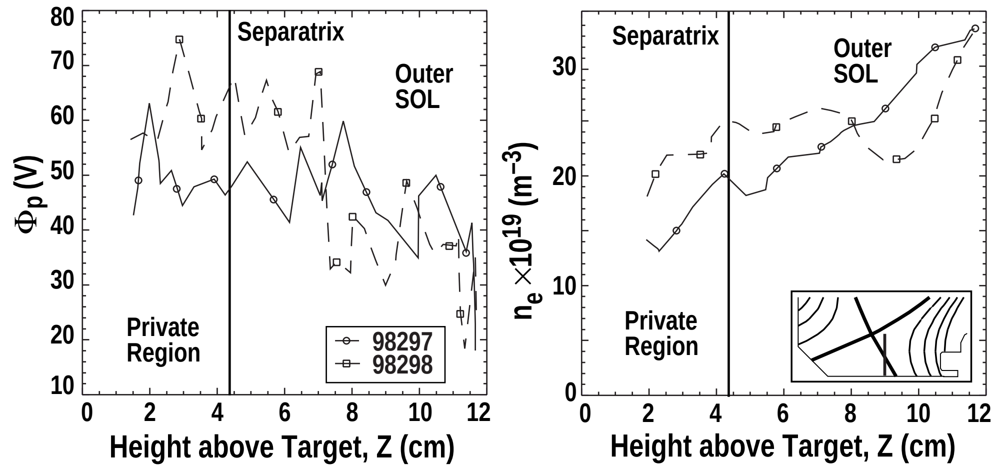


FIG. 3. Measured profiles of (a) $\Phi_p$ and (b) $n_e$ *vs*. height above target during PDD conditions for standard $B_T$.

## Discussion

Particle transport by the $\mathbf{E}\times\mathbf{B}_T$ drift is large in these discharges. The diamagnetic or $\mathbf{B}\times\nabla p/B^2$ velocity, not a true drift, transports no ions or energy [3] and is not considered here. The number of particles per second $\dot{N}$ convected poloidally by the electric drift $\mathbf{v}_E = \mathbf{E}\times\mathbf{B}/B^2 = -\nabla\Phi\times\mathbf{B}/B^2 \approx -\nabla\Phi\times\mathbf{B}_T/B_T^2$ through any axisymmetric surface defined by rotation of a curve $\ell$ and bounded by potentials $\Phi_1$ and $\Phi_2$ is:

$$\dot{N} = \int_{\ell_1}^{\ell_2} 2\pi R n\left(\mathbf{v}_E \times d\ell\right)\cdot\hat{e}_\phi \approx -2\pi\int_{\ell_1}^{\ell_2}\frac{Rn}{B_T}(\nabla\Phi)\cdot d\ell = 2\pi\int_{\Phi_2}^{\Phi_1}\frac{Rn}{B_T}d\Phi \qquad (1)$$

If $B_T$, $R$ and $n$ are all nearly constant across the potential gradient region, Eq. (1) simplifies to

$$\dot{N} \approx 2\pi R n\left(\Phi_1 - \Phi_2\right)/B_T \quad , \qquad (2)$$

and $\dot{N}$ depends on just the potential difference across the plasma flow.

For standard $B_T$ in H–mode, the electron density across the private region potential gradient region is fairly constant at $\approx 1\times10^{19}$ m$^{-3}$, Fig. 1(b), and use of Eq. (2) is justified. It yields a calculated private poloidal ion flow from the outer to the inner target region of $\dot{N} \approx 1\times10^{22}$ s$^{-1}$. For comparison, the ion flow to the outer target measured by target mounted Langmuir probes, was $\approx 2\times10^{22}$ s$^{-1}$, and ion flow to the inner target was 0.7–$2\times10^{22}$ s$^{-1}$. Thus, the private poloidal $\mathbf{E}\times\mathbf{B}_T$ flow is ~25%–40% of the total (inner plus outer) target ion flow. Particle transport with reversed $B_T$ is the same magnitude (Fig. 2) but oppositely directed. In L–mode, standard $B_T$, the private poloidal $\mathbf{E}\times\mathbf{B}_T$ ion flow was $\dot{N} \sim 1\times10^{22}$ s$^{-1}$ while the total target ion flow was ~$2\times10^{22}$ s$^{-1}$. In the PDD discharge $\dot{N} \sim 0.5$–$2\times10^{22}$ s$^{-1}$ while the total target ion flow was $\geq 2\times10^{23}$ s$^{-1}$ in the SOL and zero, within the diagnostics sensitivity, in the private region (with sensitivity). In all cases except the PDD, the $\mathbf{E}\times\mathbf{B}_T$ flow is a substantial fraction of the total flow to the target.

The private poloidal flow is supplied mainly by the radial $\mathbf{E}\times\mathbf{B}_T$ drift of plasma across the target face by the usual sheath and presheath electric field, as sketched in Fig. 4. In fact, such across–target drift appears to be the main source of private-region plasma, which is not explained by conventional divertor modeling without drifts.

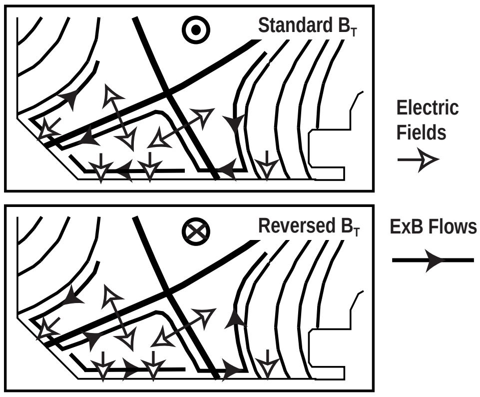


FIG. 4. Schematic of **E** and **E**×**B** directions in the divertor for standard and reversed $B_T$.

The divergence of the $n\mathbf{v}_E = n\mathbf{E}\times\mathbf{B}_T / B_T^2$ flow is not zero, due to the $R^{-1}$ dependence of $B_T$ and to local sources and sinks of $n$. The non-zero divergence is partially accommodated by plasma flow parallel to **B**.

The $\mathbf{v}_E$ particle fluxes convect a heat flux [7] $\mathbf{q}_E = n\mathbf{v}_E\left\{(5/2)k\left[T_i + (n_e/n_i)T_e\right] + e\Phi_I\right\}$, where $\Phi_I$ is the ionization potential. This equation can be integrated across the potential gradient like Eq. (1), and for approximately uniform $T_e = T_i$ and $n_e = n_i$, the convected heat flow is $Q_E \approx \dot{N}e\,(5\,T_e + \Phi_I)$ (W). For the attached, standard $B_T$, H–mode discharge, if we approximate $T_e$ by 20 eV [Fig. 1(c)] and let $\Phi_I$ = 13.6 eV (hydrogen), the poloidal private heat flow is ~0.2 MW. Measurements of heat flux to the targets by an IR camera show a total of 1.4 MW deposited onto the targets. Thus, the poloidal private flow is not important globally. However, $q_E \approx 0.48$ MW/m$^2$ is calculated just on the private side of the separatrix and is comparable to IR camera measurements of peak heat fluxes to the inner and outer targets of 0.5 MW/m$^2$ and 1.4 MW/m$^2$, respectively. Therefore, $q_E$ can be important locally.

The strength of the measured $\mathbf{E}\times\mathbf{B}_T$ flow and the agreement between computational modeling and experiment establish that $\mathbf{E}\times\mathbf{B}_T/B^2$ poloidal circulation is a main cause of the long-observed changes in divertor plasmas with the direction of $B_T$. The UEDGE simulation [2] shows private ion poloidal $\mathbf{E}\times\mathbf{B}_T$ flow of $0.5\times10^{22}$ s$^{-1}$ for standard $B_T$ direction and $0.7\times10^{22}$ s$^{-1}$ for reversed $B_T$, comparable to the experimental values. Standard 2-D divertor modeling does not include cross–$B$ drifts. Our results emphasize the need to include electric fields and drifts self-consistently in divertor modeling for interpretation of experiments, basic understanding and prediction of future divertor performance. Since **E** is generated by plasma gradients both perpendicular and parallel to **B**, this divertor $\mathbf{E}\times\mathbf{B}_T$ drift is a universal phenomena.

This research was supported by the U.S. Department of Energy under Contract Nos. DE-AC03–98ER54463, W-7405-ENG-48, DE-AC05-96OR22464, DE-AC04-94AL85000, and Grant No. DE-FG03-95ER54294. The authors acknowledge discussions with T.D. Rognlien, G.D. Porter and S.L. Allen. Special thanks to R.D. Lehmer and R.A. Moyer for their assistance during the experiments.

[1] A.V. Chankin, *et al*., Plasma Phys. Contr. Fusion **36**, (1994) 1853.
[2] T.D. Rognlien, G.D. Porter, D.D. Ryutov, J. Nucl. Mater. **266–269** (1999) 654.
[3] A.V. Chankin, J. Nucl. Mater. **241–243**, (1997) 199.
[4] S.L. Allen, *et al*., Proc. of the 17th Int. Conf. Plasma Phys. Contr. Nucl. Fusion Research, Yokohama, Japan, 1998, (International Atomic Energy Agency) to be published.
[5] L.L. Lao, *et al*., Nucl. Fusion **25**, (1985) 1611.
[6] M.J. Schaffer, *et al.,* Nucl. Fusion **37**, (1997) 83.
[7] S.I. Braginskii, Reviews of Plasma Physics, M.A. Leontovich, Editor (Consultants Bureau, New York, 1965) Vol. **1**, p. 205.